Heliyon 7 (2021) e07484

Contents lists available at ScienceDirect

Heliyon

journal homepage: www.cell.com/heliyon

Research article

Synthesis, antibacterial, anti-oxidant and molecular docking studies of imidazoquinolines

K. Velmurugan [a], Derin Don [a], Rajesh Kannan [b], C. Selvaraj [c], S. VishnuPriya [d], G. Selvaraj [e], S.K. Singh [c], R. Nandhakumar [a,*]

[a] Department of Applied Chemistry, Karunya Institute of Technology and Sciences (Deemed-to-be University), Karunya Nagar, Coimbatore, 641 114, India
[b] Department of Microbiology, Bharathidasan Univeristy, Tiruchirappalli, 620 024, India
[c] Computer Aided Drug Design and Molecular Modeling Lab, Department of Bioinformatics, Science Block, Alagappa University, Karaikudi, 630004, Tamil Nadu, India
[d] Department of Medical Neurobiology, Institute for Medical Research Israel-Canada, The Hebrew University-Hadassah Medical School, Jerusalem, 91120, Israel
[e] Centre for Interdisciplinary Sciences-Computational Life Sciences, College of Food Science and Technology, Henan University of Technology, Zhengzhou, China

ARTICLE INFO

Keywords:
Thio-imidazoquinolines
Hydroxy-imidazoquinolines
Chloro-imidazoquinolines
2-Chloro-3-formylquinolines
Antibacterial
Antioxidant
Molecular docking
Multidrug-resistant

ABSTRACT

Quinoline and imidazole derivatives have been playing a significant role in functional bioactivities and were potentially used as antibacterial, antifungal, anticancer, and anti-inflammatory drugs. Owing to the limitation of drug resistance, herein we synthesized thio-, chloro-, and hydroxyl-functionalized various imidazoquinolines by molecular hybridization approach. All the imidazoquinoline derivatives were examined for their antibacterial activity against selected bacterial pathogens by the agar well diffusion method. In addition, the anti-oxidant efficacy of imidazoquinolines was also tested using ferric reducing antioxidant power (FRAP). Among them, electron-withdrawing (-Cl) substituent containing imidazoquinoline **5f** showed higher antibacterial and anti-oxidant activities than other imidazoquinolines and reached the effectiveness of the standard. In addition, compounds **4f**, **5e**, and **3f** showed moderate antibacterial activity and other derivatives displayed weak activity against various pathogens. Molecular docking studies were also performed on selected imidazoquinoline derivatives (**3f**, **4f**, and **5f**), which showed high docking score and strong binding energy values. These results revealed that thio-imidazoquinoline could assist as a prototype for the designing of multidrug-resistant antibiotics against various microbial organisms.

1. Introduction

Bacterial infections have been vastly increased due to lack of potency with various antibiotics by strengthened antimicrobial resistance. Hence, the multidrug-resistant (MDR) bacteria is one of the major challenges in social health care [1, 2]. For example, ~2 million people acquire this MDR infection, and however, ~23,000 people decease per year [3]. At present, there is a wide range of antibacterial drugs available, even though it causes adverse side effects, such as high blood pressure, skin rashes, neuropathy, bone marrow diseases, etc [4, 5]. Also, the prolonged usage of antibiotics causes immunosuppresses of an individual. Thus, the progress of new antibiotics with enhanced toxicity is the crucial and worthwhile effort required to overcome the antibiotic resistance issue. Recently, various approaches have been implemented for the synthesis of novel antibacterial agents to overcome MDR bacteria [6, 7]. In particular, the molecular hybridization approach was implemented for the synthesis of the hybrid single molecular drug by attaching two or more bioactive pharmacophores, and thus produce fewer side effects with better efficacy. Inspired by this approach, researchers have been focusing on the synthesis of the hybrid single molecular drug by fusing both quinoline and imidazole-based pharmacophores [8]. Since quinolines and their various substituted functionalities have been stepping into the pharmacological drug activities from antiasthmatic to HIV-integrase inhibitors [9, 10, 11]. The imidazole derivatives have shown various pharmacological activities, including antihypertensive, anti-fungal, enzyme inhibition, cardiovascular activity, etc [12, 13]. These days imidazole-based antibacterial drugs, such as 1-(2-hydroxyethyl)-2-methyl-5-nitroimidazole (metronidazole) and 2-nitroimidazole (azomycin) have been used for trichomonacide applications. Also, some of the imidazoles containing vital anti-cancer drugs, such as metronidazole, clotrimazole, metrazole, and misonidazole are exploited to date. The fruitful combination of these two pharmacophores could achieve imidazoquinoline derivatives and be utilized for various

* Corresponding author.
E-mail address: nandhakumar@karunya.edu (R. Nandhakumar).

https://doi.org/10.1016/j.heliyon.2021.e07484
Received 14 April 2021; Received in revised form 26 June 2021; Accepted 1 July 2021

applications, such as modulating the phosphodiesterase and adenosine A3 receptors, high toll-like receptor 7/8 (TLR7/TLR8) selective agonists, anticancer efficacy, etc. [14, 15]. Molecular docking studies are used as a potential tool to identify the various TLR and other residues interacting with small molecular imidazoquinoline derivatives [16, 17]. As a consequence, researchers are focusing on the robust design and synthesis of imidazoquinoline derivatives with suitable functionality and can be potentially used for pharmacological and biological fields.

On the other hand, antioxidants have been playing a crucial role to inhibit the pathogenesis of various chronic diseases. Such diseases were caused by the processes of generating various reactive oxygen species [ROS] and also the release of free radicals from oxidative injuries. These oxidative injuries are associated with radiation [18], food components, or pollution or which are produced endogenously by metabolic reactions in the human body [19] accountable for oxidative damage to proteins, DNA, and lipids [20]. Many experiments showed that antioxidants could be potent in inhibiting or overcoming such disorders [21]. Hence, the synthesized imidazoquinolines-based free radical scavenging activity occurs either from phenolic –OH or –SH groups of the quinoline moiety. Therefore, a free radical can abstract an H atom or can undergo electron transfer from these sites. Nevertheless, literature reports have supported it to the phenolic -OH group [22]. Based on the above interest, we have synthesized some new heterocyclic fused systems, which comprised of both quinolines and imidazoles together via the classical Vilsmeier-Haack reaction. This reaction is utilized for developing many synthetic methodologies as an efficient reaction for the reactive aromatic and heteroaromatic formylation, respectively [23]. Accordingly, we have synthesized the 2-chloro-3-formyl quinoline via the Vilsmeier-Haack reaction followed by cyclization in the presence of orthophenylenediamine (OPD) [24]. Herein, we synthesized the series of imidazoquinoline derivatives (Figure 1) and screened their antibacterial activity and molecular docking. In addition, the radical scavenging activity of the imidazoquinolines was studied by screening their reducing ability of FRAP assay.

2. Results and discussion

The precursor 2-chloro-3-formylquinoline (**1a)** was synthesized by the classical Vilsmeier-Haack reaction on acetanilide according to the earlier reported procedure [25]. The prepared compound was then treated with 4N HCl to obtain the 3-formyl-2-hydroxyquinoline **2a**. This intermediate compound **2a** was further treated with OPD in the presence of triethylamine in ethanol under reflux condition for 10 h obtained the compound **3a** in 80% Yield (m.p. 251–253 °C). IR spectrum of **3a** showed strong absorption peaks at 1606, 1654, and 3342 cm^{-1}, which corresponds to C=N, amide, and –NH groups [26]. The ^1H NMR spectrum of **3a** showed that two singlets at δ 12.65 and 12.47 ppm accountable for the –OH of quinoline and –NH of the imidazole scaffolds, respectively. A fine singlet at δ 9.11 ppm was attributed to the C_4–H of the quinoline. The rest of the eight aromatic protons resonances showed their signals between δ 7.73 and 7.18 ppm as multiplets. The elemental analysis was also corroborated with the proposed molecular formula $C_{16}H_{11}N_3O$ and the mass spectra displayed the molecular ion peak at m/z: $[M^+ + H]^+$ 262. All the above studies were supported that compound **3a** as 3-(1*H*-benzo[*d*] imidazole-2-yl)quinolin-2-ol. Earlier, we aimed to obtain a dimer product by using an excess of 2-hydroxy-3-formyl quinoline in the reaction. Surprisingly, we end up only in the formation of imidazoquinolines even taking excess of 2-hydroxy-3-formyl quinoline for this reaction. Therefore, the same reaction procedures were extended to its derivatives **2(b-f)** with OPD, and their products **3(b-f)** were confirmed by various spectral and analytical studies.

After preparing the oxo-derivatives, we envisaged the preparation of its chloro- and thio-analogues. Accordingly, the same precursor 2-chloro-3-formylquinoline **1a** was mixed with OPD in the presence of triethylamine in ethanol under reflux condition for 10 h obtained the chloro-derivative of the imidazoquinoline **4a** in 84% Yield. (m.p. 201–203 °C) and its IR spectra showed three peaks at 741, 1615, and 3364 cm^{-1} corresponds to C–Cl, C=N, and –NH groups. Its ^1H NMR spectrum represented a broad singlet at δ 10.59 ppm for the imidazole –NH proton. A fine singlet at δ 9.26 ppm was attributed to the C_4–H of the quinoline. The rest of the quinoline and imidazole aromatic protons showed their multiplet between δ 8.03 and 7.38 ppm. The mass spectrum gave the molecular ion peak at m/z: $[M^+]^+$ 279 and the CHN analysis showed its molecular formula as $C_{16}H_{10}ClN_3$. The above details including the analytical data confirmed that compound **4a** as 3-(1*H*-benzo[*d*]imidazole-2-yl)-2-chloroquinoline. Subsequently, compound **4a** was treated with sodium sulphide in the presence of dimethylformamide under room temperature stirring for 5 h to obtain the thio-derivative of imidazoquinoline **5a** in 82% Yield as yellow colour solid. (m.p. 204–205 °C) and its

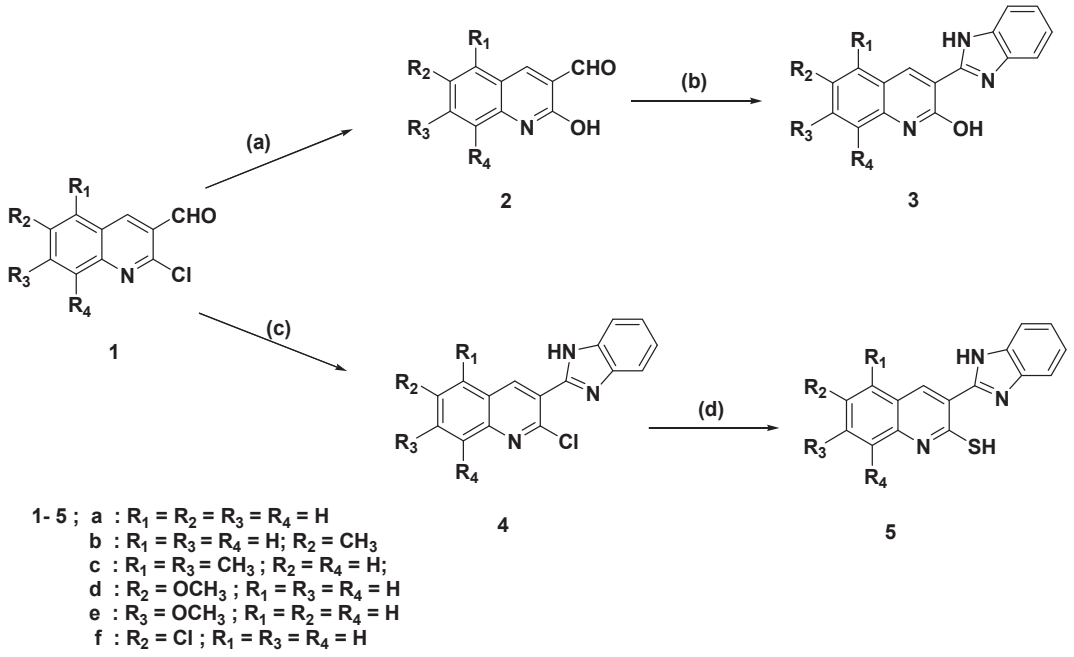

Figure 1. Synthesis of various imidazoquinolines. (a) 4N HCl, reflux, 4h, (b) & (c) OPD, TEA, EtOH, reflux, 10 h, (d) Na_2S, DMF, RT, Stir, 5 h.

IR spectra showed two peaks at 1658 (C=N) and 3444 cm^{-1} (N–H). The ^1H NMR spectra of the compound showed a multiplet δ 8.00–7.27 ppm for the eight aromatic proton resonances for the quinoline and imidazole moieties. It also exhibited a sharp singlet and a broad singlet at δ 9.19 and 14.18 ppm for the quinoline C_4–H and quinoline –SH protons, respectively. The molecular formula $C_{16}H_{11}N_3S$ was confirmed from its analytical data and the mass spectra showed its peak at m/z: $[M^+ + H]^+$ 278.07.

The same reaction conditions were performed on **1(b-f)** with OPD and also **4(b-f)** with sodium sulphide and got the expected products **4(b-f)** and **5(b-f)**. All the newly synthesized imidazoquinolines were well characterized by the usual spectroscopic and analytical studies.

2.1. Biological evaluation

2.1.1. Antibacterial activity

The newly synthesized imidazoquinolines **3–5(a-f)** were examined for their *in vitro* antibacterial activities against the seven bacterial strains namely, *S. aureus, A. hydrophila, E. coli, K. pneumonia, S. paratyphi, S. typhi,* and *M. butyricum* by the agar well diffusion method using Ofloxacin as the control. The nutrient agar was used to culture the bacterial strains and DMSO (solvent) was used as a negative control. The susceptibility was measured based on the zone of inhibition (in diameter) against various bacterial strains. The antibacterial activity results exhibited that most of the imidazoquinolines displayed diverging degrees of inhibition against various bacterial strains. The zone of inhibition measured in mm (diameter) is compared to the current antimicrobial drug Ofloxacin as shown in Figure 2. These results revealed that most of the imidazoquinoline derivatives flourished activity against almost all the pathogenic bacteria. Although all the thio-derivatives of imidazoquinolines **5(a-f)** showed noteworthy inhibition effect on the bacterial growth. In particular, compound **5f** showed high activity and almost reached the effectiveness of the control. Notably, a 10-fold excess concentration of **5f** (100 mg/disc) displayed higher antibacterial activity to *E. coli*, *K. pneumonia, S. paratyphi, S. typhi, M. butyricum* than that of in standard (10 mg/disc). This may be due to the thio- and chloro-pharmacophores present in the **5f** molecule. In the case of chloro-imidazoquinolines **4(a–f)**, **4f** showed moderate activity against all bacterial strains, possibly due to the two electronegative chlorine atoms present in the quinoline ring of the **4f**. Similarly, among the oxo-derivatives of imidazoquinolines **3(a-f)**, compound **3f** exhibited moderate activity against all pathogens in comparison to other analogues. This may be due to the chlorine atom and the hydroxyl groups present in the **3f** molecule. However, at low concentrations i.e., 10 mg/disc some of the derivatives of the synthesized imidazoquinolines (**3(a-e)** and **4(a-c)**) had less significant activity. Finally, on comparing the oxo-, chloro-, and thio-derivatives of the imidazoquinolines, the thio-scaffolds showed prominent antibacterial activities and the pharmacore chloro-group plays a key role in improving their activity in dose-dependent.

Based on the above results, some of the selected imidazoquinolines (**3f**, **4e**, **4f**, **5e,** and **5f**) were further analyzed for their minimum inhibitory concentration (MIC) and minimal bactericidal concentrations (MBC). In Figure 3, compounds **5f** showed better MIC activity against *S. aureus*, *A. hydrophila,* and *S. typhi*. Similarly, **5f** exhibited better MBC activity against *S. aureus*, *E. coli,* and *K. pneumonia*.

To examine the SAR studies [27, 28]:

1. Electron withdrawing group (-Cl) on the quinoline ring of **5f** showed maximum antibacterial activity than other imidazoquinolines and reached the effectiveness of the standard. At high concentration (100 mg/disc), **5f** demonstrated the higher activity against *E. coli, K. pneumonia, S. paratyphi, S. typhi, M. butyricum* than that of in standard (10 mg/disc). In addition, other electron-withdrawing substituents containing compounds **4f** and **3f** also exhibited moderate activity.
2. Electron donating groups (-OCH_3) on the quinoline ring of **5e** displayed a moderate activity than other imidazoquinolines containing similar substituents (**4e** and **3e**).
3. Chloro- and thio-imidazoquinolines of **4-5(a-d)** also achieved moderate activity than that of in hydroxyl-imidazoquinolines of **3(a-e).**
4. For overall comparison, the order of antibacterial activities of imidazoquinolines was shown here, **5f** > **4f** > **5e** > **3f** > **4e** > **4d** ≈ **4a** ≈ **5b** ≈ **5d** > **5c** > **5a** ≈ **4c** ≈ **4b** > **3e** > **3d** > **3b** ≈ **3c** > **3a**.

2.1.2. Antioxidant activity using FRAP assay

The reduction of ferric (Fe^{3+}) to ferrous (Fe^{2+}) ion in the presence of antioxidants could be measured by using FRAP assay. Based on the synthesized compounds reducing capacity, which could function as a substantial sign of its potent antioxidant activity [29]. Figure 4 reveals that compound **5f** showed higher ferric reducing power than other compounds. This obtained value of the thio-functionalized imidazoquinoline **5f** was comparable to that of the standard butylated hydroxytoluene (BHT). The remaining compounds in series **5a-e** also displayed good to moderate activity. In general, the reducing power of the thio-functionalized derivatives **(5(a-f))** was relatively higher than the hydroxyl-functionalized derivatives **(3(a-f))**. Though, **3 (a-f)** showed a higher reducing power than the chloro-functionalized imidazoquinolines **(4(a-f))**. Therefore, the order of the reducing power of imidazoquinolines are **5(a-f)** > **3(a-f)** > **4(a-f)**. From these results, it is assumed that in this assay the substitutions at the C_2 positions (-OH, -Cl, and –SH) and C_6 position in the quinoline moiety, as well as the heteroatoms incorporated in the imidazole scaffold, might play substantial roles in suppressing the radicals.

2.2. Molecular docking studies

Imidazoquinoline derivatives (**3f**, **4f,** and **5f**) have a greater tendency to interact with taken seven proteins, including *S. aureus* tyrosyl-tRNA synthetase (1JIJ), *E. coli*-DNA gyrase B (1EI1), *K. pneumoniae* (4OR7), *A. hydrophila* PROAEROLYSIN (1PRE), *S. paratyphi* lipopolysaccharide acetyltransferase periplasmic domain (6SE1), *S. typhi* CDP-D-glucose 4, 6-dehydratase (1WVG), and *M. tuberculosis* MTB phosphotyrosine phosphatase B protein (2OZ5). These compound tendencies were evaluated based on the scoring values determined from the ligand-binding efficiency with protein. Particularly, **3f**, **4f,** and **5f** showed the higher scoring values with 4OR7 (∼-7 kcal/mol) and 2OZ5 (∼-5 to -7 kcal/mol) proteins, respectively which is due to hydrogen bonding and π-π interactions. Conversely, these ligands exhibited the least scoring values with 1PRE (∼-3.2 to -3.6 kcal/mol) and 6SE1 proteins (∼-2.94 to -5.34 kcal/mol), respectively, even though docking scores are in the acceptable range. Especially, the docking energy and binding energy of these ligands with 1PRE and 6SE1 proteins showed higher values because of their hydrogen bonding and more numbers of π-π and π-cation interactions. The simulated binding energies revealed that all derivatives formed a stable complex with proteins. Briefly, **3f**, **4f,** and **5f** displayed the strongest binding with 1JIJ, 1EI1, and 2OZ5, respectively based on its lowest energy values (∼-40.00 kcal/mol). Also, the other proteins exhibited various binding energies ranged between ∼ -25 to -30 kcal/mol, demonstrating that there was favorable binding with ligands. The detailed scoring values, hydrogen bonding, π-π, and π-cation interactions were shown in Table 1 and Figures 5, 6, and 7. Interestingly, the hydrogen bond, π-π interactions, and π-cation interactions were seen in **3f**, **4f,** and **5f** bound with 1PRE, 6SE1, and 2OZ5, respectively.

For comparative analysis, the ligands bound with the following crystal structure complexes (PDB ID's 1JIJ, 1EI1, 1WVG, 2OZ5, and 4OR7) were separated and re-docked with the same grid to ensure the quality, scoring, and molecular interactions (Table 2 and Figure 8). The imidazoquinoline derivatives showed prominent and strong binding interactions with low energy profiles compared to the ligands that existed in the crystal structures. These results indicated that the imidazoquinoline derivatives are the potential inhibitors to the selected targets.

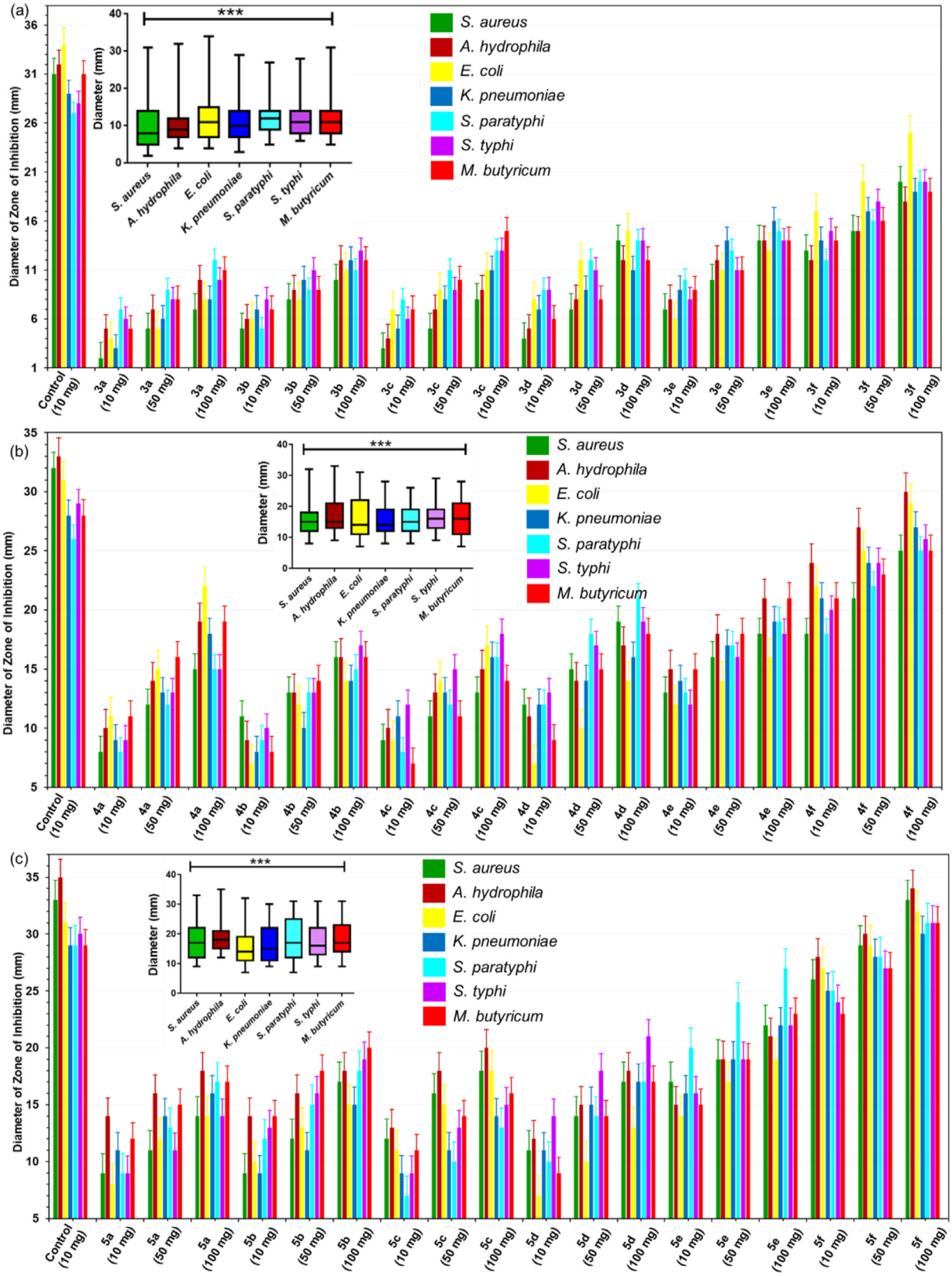

Figure 2. *In vitro* antibacterial activity of imidazoquinoline derivatives by disc-diffusion assay. (a) **3(a–f)** (mg/disc), (b) **4(a–f)** (mg/disc), (c) **5(a–f)** (mg/disc). Ofloxacin was used as a control and error bars represent the standard deviation (SD) from three independent analyses. Insets show the statistical analysis of the differences between zone of inhibitions of all compounds **3–5(a-f)**. Analyzed results are displayed as mean ± SD (**p* value: 0.05–0.01; ***p* value: <0.001; ****p* value: <0.0001).

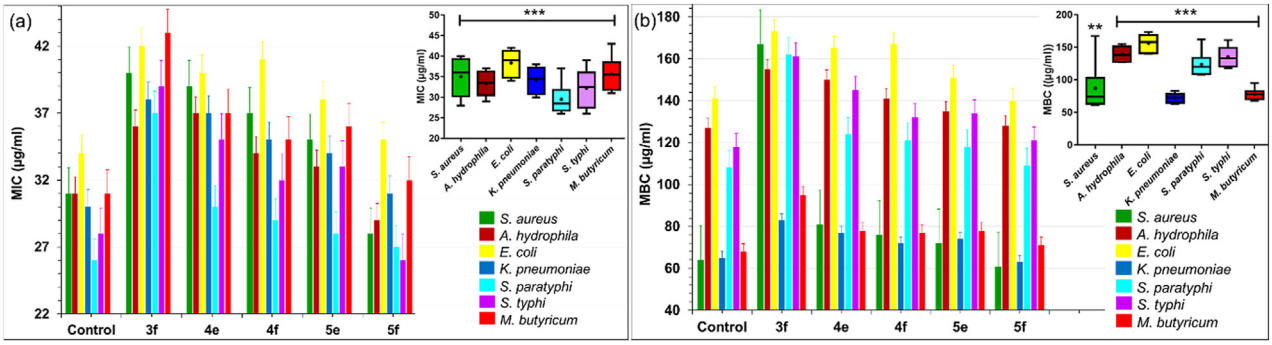

Figure 3. (a, b) MIC and MBC of the selected imidazoquinolines (**3f, 4e, 4f, 5e**, and **5f**) were compared with standard Ofloxacin. Error bars represent the SD from three independent analyses. Insets show the MIC and MBC of selected bacterial strains activity against imidazoquinolines (**3f, 4e, 4f, 5e** and **5f**). Results are presented as mean ± SD (*p value: 0.05–0.01; **p value: <0.001; ***p value: <0.0001).

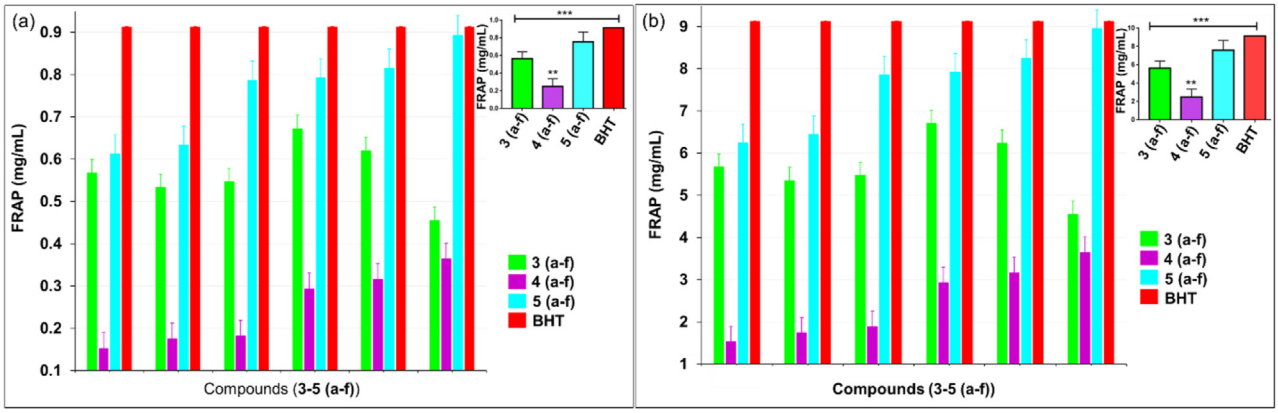

Figure 4. Anti-oxidant activity of imidazoquinolines **3–5(a–f)**, (a) 1 mg/mL, (b) 10 mg/mL. BHT acts as a control and error bars represent the SD of three independent analyses. Insets shows the anti-oxidant activity of **3-5(a–f)** against the FRAP. Values are mean of three determinations, the ranges of which are mean ± SD (*p value: 0.05–0.01; **p value: <0.001; ***p value: <0.0001).

3. Experimental section

3.1. Synthesis of imidazoquinolines

Compounds **1** and **2** were prepared according to the reported literature [30].

Synthesis of 3: Appropriate 2-hydroxyquinoline-3-carbaldehyde (2.89 mmol), *o*-phenylenediamine (3.17 mmol) were mixed with ethanol (20 mL) in the presence of triethylamine (4.33 mmol) and refluxed for ten hours. After that, the obtained precipitate was filtered and recrystallized from ethanol to give compound **3.**

Compound 3a: Yellow colour Solid (80% yield). M.p.: 251–253 °C; ^{1}H NMR (400 MHz, DMSO-d_6) δ: 12.65 (s, 1H, OH), 12.47 (s, 1H, NH), 9.11 (s, 1H, Ar), 7.95–7.97 (d, J = 8 Hz, 1H, Ar), 7.59–7.73 (m, 3H, Ar), 7.43–7.45 (d, J = 8 Hz, 1H, Ar), 7.29–7.32 (t, J = 10 Hz, 1H, Ar), 7.18–7.23 (m, 2H, Ar) ppm; ^{13}C NMR (125 MHz, DMSO-d_6) δ: 113.2, 115.7, 118.7, 119.6, 120.4, 122.3, 122.7, 123.1, 129.5, 132, 134.9, 139.1, 139.5, 143.2, 148.1, 161.2 (C=N) ppm. Elemental analysis: Anal. calc. for: $C_{16}H_{11}N_3O$: C, 73.55; H, 4.24; N, 16.08%. Found: C, 73.48; H, 4.21; N, 16.02%. LC-MS calcd. for $C_{16}H_{11}N_3O$: [M^+] 261, found [M^++H]$^+$ 262.

Compound 3b: (88% yield). M.p.: 235–237 °C; ^{1}H NMR (400 MHz, DMSO-d_6) δ: 12.67 (s, 1H, OH), 12.42 (s, 1H, NH), 9.12 (s, 1H, Ar), 7.98–8.00 (d, J = 8 Hz, 1H, Ar), 7.45–7.72 (m, 3H, Ar), 7.16–7.26 (m, 3H, Ar), 2.41 (s, 3H, CH_3) ppm; ^{13}C NMR (125 MHz, DMSO-d_6) δ: 22.4, 114.3, 116.2, 117.4, 119.2, 120.5, 122.7, 122.3, 123.4, 129.6, 132.1, 134.6, 139.3, 139.8, 143.5, 148.6, 161.9 (C=N) ppm. Elemental analysis: Anal. calc. for: $C_{17}H_{13}N_3O$: C, 74.17; H, 4.76; N, 15.26%. Found: C, 74.08; H, 4.82; N, 15.28%. LC-MS calcd. for $C_{17}H_{13}N_3O$: [M^+] 275, found [M^++H]$^+$ 276.

Compound 3c: (82% yield). M.p.: 231–233 °C; ^{1}H NMR (400 MHz, DMSO-d_6) δ: 12.62 (s, 1H, OH), 12.43 (s, 1H, NH), 9.15 (s, 1H, Ar), 7.96–7.98 (d, J = 8 Hz, 1H, Ar), 7.52–7.74 (m, 3H, Ar), 7.19–7.24 (m, 2H, Ar), 2.46 (s, 3H, CH_3), 2.42 (s, 3H, CH_3) ppm; ^{13}C NMR (125 MHz, DMSO-d_6) δ: 22.3, 22.7, 112.8, 115.2, 119.3, 119.8, 121.2, 122.8, 123.1, 123.4, 129.9, 131.9, 135.2, 139.3, 139.8, 144.2, 148.7, 161.9 (C=N) ppm. Elemental analysis: Anal. calc. for: $C_{18}H_{15}N_3O$: C, 74.72; H, 5.23; N, 14.52%. Found: C, 74.83; H, 5.26; N, 14.48%. LC-MS calcd. for $C_{18}H_{15}N_3O$: [M^+] 289, found [M^++2H] $^+$ 291.

Compound 3d: (78% yield). M.p.: 201–203 °C; ^{1}H NMR (400 MHz, DMSO-d_6) δ: 12.62 (s, 1H, OH), 12.49 (s, 1H, NH), 9.13 (s, 1H, Ar), 7.97–7.99 (d, J = 8 Hz, 1H, Ar), 7.50–7.74 (m, 3H, Ar), 7.20–7.32 (m, 3H, Ar), 3.91 (s, 3H, OCH_3) ppm; ^{13}C NMR (125 MHz, DMSO-d_6) δ: 54.2, 113.6, 115.9, 118.5, 119.8, 120.6, 122.5, 122.6, 123.3, 129.6, 132.2, 135.2, 139.4, 139.7, 143.6, 148.3, 161.5 (C=N) ppm. Elemental analysis: Anal. calc. for: $C_{17}H_{13}N_3O_2$: C, 74.17; H, 4.76; N, 15.26%. Found: C, 74.12; H, 4.78; N, 15.30%. LC-MS calcd. for $C_{17}H_{13}N_3O_2$: [M^+] 291, found [M^++2H]$^+$ 293.

Compound 3e: (79% yield). M.p.: 211–213 °C; ^{1}H NMR (400 MHz, DMSO-d_6) δ: 12.64 (s, 1H, OH), 12.48 (s, 1H, NH), 9.14 (s, 1H, Ar), 7.94–7.96 (d, J = 8 Hz, 1H, Ar), 7.52–7.75 (m, 3H, Ar), 7.19–7.26 (m, 3H, Ar), 3.92 (s, 3H, OCH_3) ppm; ^{13}C NMR (125 MHz, DMSO-d_6) δ: 53.4, 114.1, 116.2, 119.3, 119.9, 121.3, 123.2, 123.1, 123.8, 130.2, 132.8, 135.1, 139.6, 140.2, 143.7, 148.7, 161.8 (C=N) ppm. Elemental analysis:

Table 1. Molecular docking scores of **3f**, **4f,** and **5f** with various proteins are obtained *via* Glide docking.

	1JIJ	1EI1	4OR7	1PRE	6SE1	1WVG	2OZ5
Docking Score (kcal/mol)							
3f	-5.856	-5.75	-7.092	-3.254	-5.34	-5.681	-7.09
4f	-4.746	-5.62	-7.271	-3.527	-4.085	-4.522	-4.998
5f	-3.719	-5.50	-7.333	-3.658	-2.944	-5.036	-7.087
Docking Energy (kcal/mol)							
3f	-42.631	-42.15	-38.027	-32.417	-21.946	-38.217	-30.993
4f	-38.106	-42.13	-34.736	-28.773	-20.645	-35.474	-34.333
5f	-47.912	-41.51	-36.696	-29.34	-9.108	-40.007	-31.662
Glide Emodel (kcal/mol)							
3f	-60.326	-57.34	-46.985	-39.417	-5.063	-45.29	-41.582
4f	-54.606	-56.20	-44.643	-38.413	-3.656	-36.034	-43.70
5f	-62.649	-56.24	-47.257	-36.846	-2.327	-36.596	-44.246
Binding Energy (MM/GBSA) kcal/mol							
3f	-27.94	-46.9	-32.86	-40.8	-27.04	-30.42	-40.60
4f	-40.16	-47.25	-33.43	-34.13	-24.9	-31.31	-40.22
5f	-40.16	-51.33	-31.24	-31.34	-25.44	-29.08	-45.01
Number of Hydrogen Bonds							
3f	2	1	1	1	2	1	1
4f	1	0	1	1	1	0	0
5f	2	1	1	1	0	1	1
π-π and π-cation Interactions (Numbers)							
3f	0	0	0	1	3	0	2
4f	0	0	0	1	3	0	0
5f	0	0	0	0	2	0	2

Anal. calc. for: $C_{17}H_{13}N_3O_2$: C, 70.09; H, 4.50; N, 14.42%. Found: C, 69.89; H, 4.48; N, 14.48%. LC-MS calcd. for $C_{17}H_{13}N_3O_2$: $[M^+]$ 291, found $[M^++H]^+$ 292.

Compound 3f: (71% yield). M.p.: 202–204 °C; ^{1}H NMR (400 MHz, DMSO-d_6) δ: 12.68 (s, 1H, OH), 12.52 (s, 1H, NH), 9.17 (s, 1H, Ar), 7.98–8.00 (d, J = 8 Hz, 1H, Ar), 7.55–7.78 (m, 3H, Ar), 7.21–7.32 (m, 3H, Ar) ppm; ^{13}C NMR (125 MHz, DMSO-d_6) δ: 114.3, 116.2, 119.4, 120.1, 120.8, 122.9, 123.2, 123.7, 130.0, 132.6, 135.3, 140.3, 140.5, 143.9, 148.7, 161.8 (C=N) ppm. Elemental analysis: Anal. calc. for: $C_{16}H_{10}N_3O$: C, 64.98; H, 3.41; N, 14.21%. Found: C, 65.06; H, 3.43; N, 14.18%. LC-MS calcd. for $C_{16}H^{35}_{10}ClN_3O$: $[M^+]$ 295, found $[M^++2H]^+$ 297; calcd. for $C_{16}H^{37}_{10}ClN_3O$: $[M^+]$ 297, found $[M^++2H]^+$ 299.

Synthesis of 4: *o*-phenylenediamine (1.15 mmol) treated with 2-chloroquinoline-3-carbaldehyde **3** (1.04 mmol) in ethanol (20 mL) and triethylamine (1.56 mmol), and refluxed for ten hours. The obtained precipitate was recrystallized from chloroform to afford compound **4.**

Compound 4a: White solid in 84% yield. M.p.: 201–203 °C; ^{1}H NMR (400 MHz, $CDCl_3$) δ: 10.59 (bs, 1H, NH), 9.26 (s, 1H, Ar), 8.03–8.05 (d, 1H, Ar), 7.92–7.94 (d, J = 8 Hz, 1H, Ar), 7.79–7.83 (m, 2H, Ar), 7.60–7.64 (m, 2H, Ar), 7.27–7.38 (m, 2H, Ar) ppm. ^{13}C NMR (125 MHz, $CDCl_3$) δ: 110.7, 117.9, 119.4, 122.6, 123.3, 125.6, 125.7, 127.9, 128.1, 130.4, 139.3, 143.5, 147.1, 150.0, 159.8 (C=N) ppm. Elemental analysis: Anal. calcd. for: $C_{16}H_{10}ClN_3$: C, 68.70; H, 3.60; N, 15.02%. Found: C, 68.64; H, 3.52; N, 14.98%. LC-MS calcd. for $C_{16}H^{35}_{10}ClN_3$: $[M^+]$ 279, found $[M^+]$ 279; calcd. for $C_{16}H^{37}_{10}ClN_3$: $[M^+]$ 281, found $[M^+]$ 281 [31].

Compound 4b: 88% yield. M.p.: 179–181 °C; ^{1}H NMR (400 MHz, $CDCl_3$) δ: 10.61 (bs, 1H, NH), 9.28 (s, 1H, Ar), 8.04–8.06 (d, J = 8 Hz, 1H, Ar), 7.94–7.96 (d, J = 8 Hz, 1H, Ar), 7.65–7.78 (m, 3H, Ar), 7.26–7.32 (m, 2H, Ar), 2.42 (s, 3H, CH_3) ppm. ^{13}C NMR (125 MHz, $CDCl_3$) δ: 22.6, 110.2, 118.2, 119.6, 122.3, 123.1, 125.8, 125.9, 127.1, 128.5, 130.3, 139.6, 143.4, 147.3, 150.6, 159.9 (C=N) ppm. Elemental analysis: Anal. calcd. for: $C_{17}H_{12}ClN_3$: C, 69.51; H, 4.12; N, 14.30%. Found: C, 69.56; H, 4.10; N, 14.36%. LC-MS calcd. for $C_{17}H^{35}_{12}ClN_3$: $[M^+]$ 293, found $[M^++H]^+$ 294; calcd. for $C_{17}H^{37}_{12}ClN_3$: $[M^+]$ 295, found $[M^++H]^+$ 296.

Compound 4c: 81% yield. M.p.: 209–211 °C; ^{1}H NMR (400 MHz, $CDCl_3$) δ: 10.63 (bs, 1H, NH), 9.28 (s, 1H, Ar), 8.02–8.04 (d, J = 8 Hz, 1H, Ar), 7.85–7.96 (m, 2H, Ar), 7.32–7.45 (m, 3H, Ar), 2.47 (s, 3H, CH_3), 2.44 (s, 3H, CH_3) ppm. ^{13}C NMR (125 MHz, $CDCl_3$) δ: 22.5, 22.9, 110.7, 118.4, 120.6, 122.8, 123.7, 125.9, 126.2, 127.4, 129.6, 130.4, 138.2, 144.6, 147.7, 150.9, 160.5 (C=N) ppm. Elemental analysis: Anal. calcd. for: $C_{18}H_{14}ClN_3$: C, 70.24; H, 4.58; N, 13.65%. Found: C, 70.29; H, 4.53; N, 13.88%. LC-MS calcd. for $C_{18}H^{35}_{14}ClN_3$: $[M^+]$ 307, found $[M^++2H]^+$ 309; calcd. for $C_{18}H^{37}_{14}ClN_3$: $[M^+]$ 309, found $[M^++2H]^+$ 311.

Compound 4d: 89% yield. M.p.: 190–194 °C; ^{1}H NMR (400 MHz, $CDCl_3$) δ: 10.64 (bs, 1H, NH), 9.29 (s, 1H, Ar), 8.07–8.09 (d, J = 8 Hz, 1H, Ar), 7.76–7.89 (m, 2H, Ar), 7.32–7.45 (m, 4H, Ar), 3.92 (s, 3H, OCH_3) ppm. ^{13}C NMR (125 MHz, $CDCl_3$) δ: 54.7, 111.2, 119.1, 121.5, 122.4, 123.9, 124.3, 126.1, 127.8, 129.7, 131.6, 138.7, 145.8, 147.5, 149.3, 160.1 (C=N) ppm. Elemental analysis: Anal. calcd. for: $C_{17}H_{12}ClN_3O$: C, 65.92; H, 3.90; N, 13.57%. Found: C, 65.96; H, 3.87; N, 13.48%. LC-MS calcd. for $C_{17}H^{35}_{12}ClN_3O$: $[M^+]$ 309, found $[M^+]$ 309; calcd. for $C_{17}H^{37}_{12}ClN_3O$: $[M^+]$ 311, found $[M^+]$ 311.

Compound 4e: 86% yield. M.p.: 237–239 °C; ^{1}H NMR (400 MHz, $CDCl_3$) δ: 10.62 (bs, 1H, NH), 9.28 (s, 1H, Ar), 8.04–8.06 (d, J = 8 Hz, 1H, Ar), 7.83–7.95 (m, 2H, Ar), 7.42–7.65 (m, 4H, Ar), 3.94 (s, 3H, OCH_3) ppm. ^{13}C NMR (125 MHz, $CDCl_3$) δ: 53.8, 111.8, 117.5, 119.6, 122.9, 123.4, 125.8, 126.2, 127.8, 128.7, 130.4, 138.6, 143.9, 147.7, 150.3, 159.2 (C=N) ppm. Elemental analysis: Anal. calcd. for: $C_{17}H_{12}ClN_3O$: C, 65.92; H, 3.90; N, 13.57%. Found: C, 65.98; H, 3.87; N, 13.68%. LC-MS calcd. for $C_{17}H^{35}_{12}ClN_3O$: $[M^+]$ 309, found $[M^++H]^+$ 310; calcd. for $C_{17}H^{37}_{12}ClN_3O$: $[M^+]$ 311, found $[M^++H]^+$ 312.

Compound 4f: 72% yield. M.p.: 167–171 °C; ^{1}H NMR (400 MHz, $CDCl_3$) δ: 10.64 (bs, 1H, NH), 9.29 (s, 1H, Ar), 8.06–8.09 (d, J = 12 Hz, 1H, Ar), 7.83–7.95 (m, 2H, Ar), 7.32–7.46 (m, 4H, Ar) ppm. ^{13}C NMR (125 MHz, $CDCl_3$) δ: 111.2, 118.4, 119.7, 122.9, 123.6, 125.8, 126.4, 127.8, 128.6, 130.7, 139.8, 143.8, 148.7, 150.9, 159.3 (C=N) ppm. Elemental analysis: Anal. calcd. for: $C_{16}H_9Cl_2N_3$: C, 61.17; H, 2.89; N, 13.38%. Found: C, 61.23; H, 2.85; N, 13.45%. LC-MS calcd. for $C_{16}H^{35}_9Cl_2N_3$: $[M^+]$ 314, found $[M^++2H]$ 316; calcd. for $C_{16}H^{35}_9Cl^{37}ClN_3$:

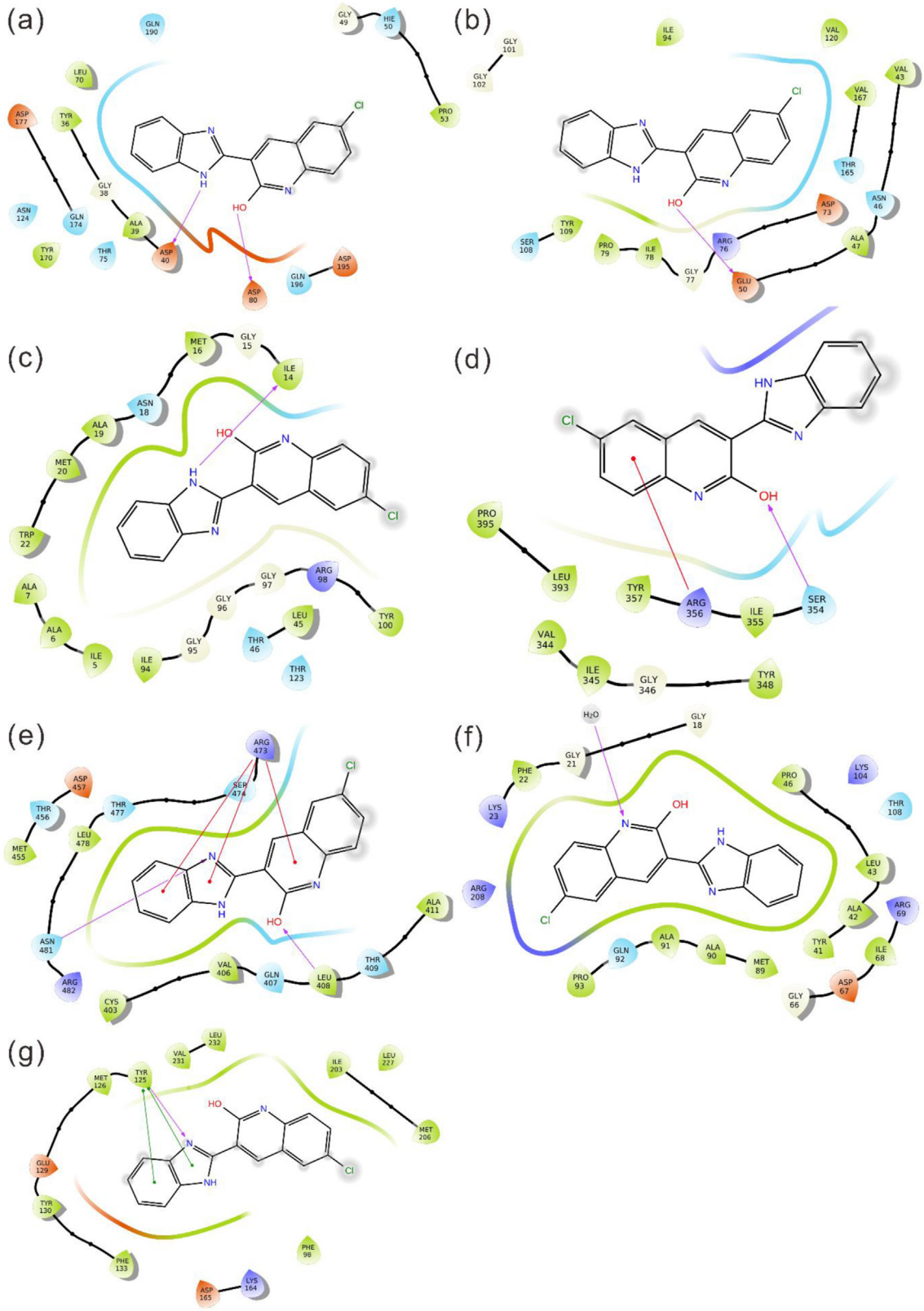

Figure 5. Docking interaction between imidazoquinoline derivative **3f** and selected targets; a) **3f**-1JIJ complex; b) **3f**-1EI1 complex; c) **3f**-4OR7 complex; d) **3f**-1PRE complex; e) **3f**-6SE1 complex; f) **3f**-1WVG complex; g) **3f**-2OZ5 complex. Hydrogen bonding (pink arrow), π-π stacking (green arrow), and π-cation (red arrow).

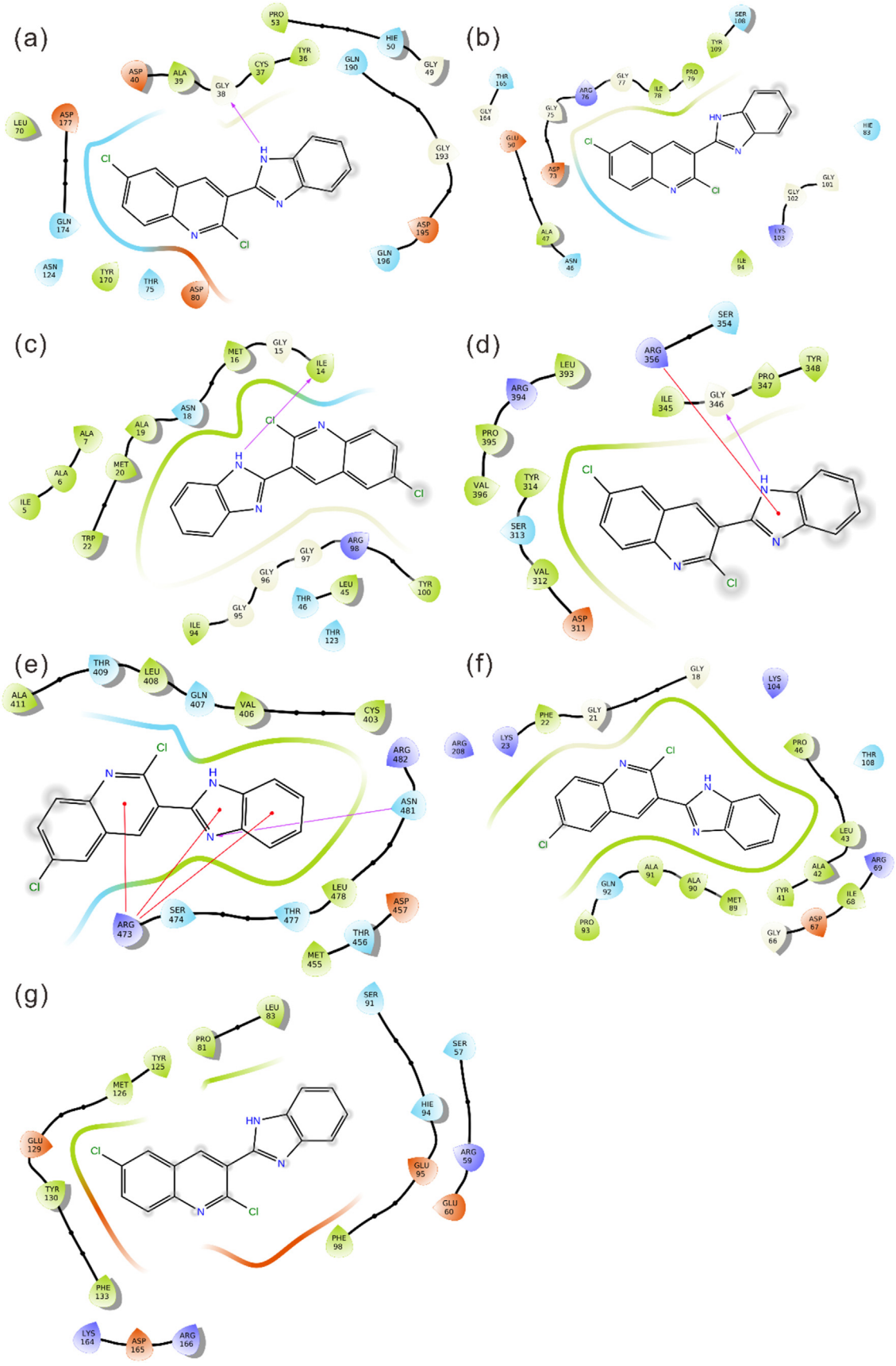

Figure 6. Docking interaction between imidazoquinoline derivative **4f** and selected targets; a) **4f**-1JIJ complex; b) **4f**-1EI1 complex; c) **4f**-4OR7 complex; d) **4f**-1PRE complex; e) **4f**-6SE1 complex; f) **4f**-1WVG complex; g) **4f**-2OZ5 complex. Hydrogen bonding (pink arrow), π-π stacking (green arrow), and π-cation (red arrow).

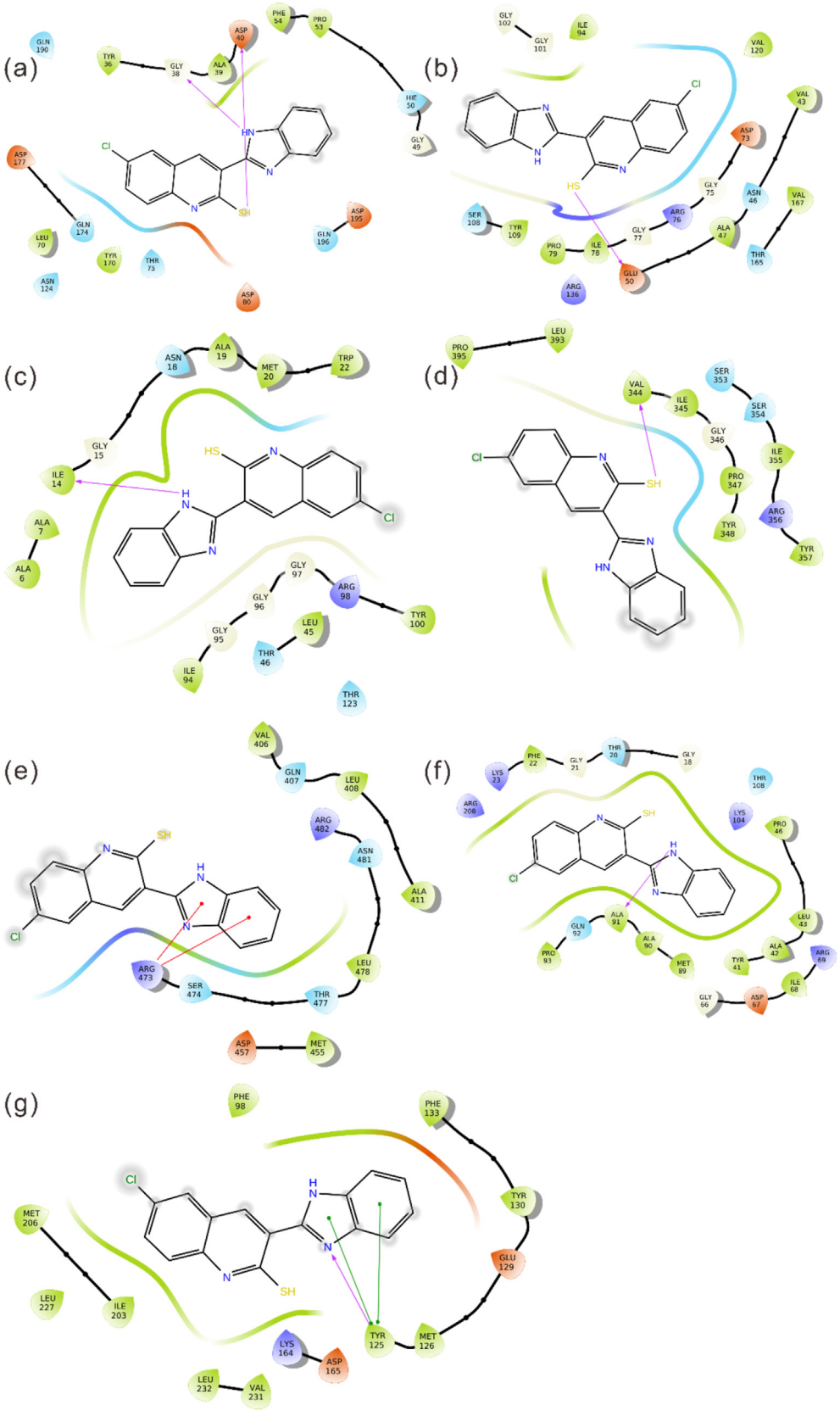

Figure 7. Docking interaction between imidazoquinoline derivative **5f** and selected targets; a) **5f**-1JIJ complex; b) **5f**-1EI1 complex; c) **5f**-4OR7 complex; d) **5f**-1PRE complex; e) **5f**-6SE1 complex; f) **5f**-1WVG complex; g) **5f**-2OZ5 complex. Hydrogen bonding (pink arrow), π-π stacking (green arrow), and π-cation (red arrow).

Table 2. Re-docking profiles of crystal bound ligands taken for the study with XP docking methodology.

PDB ID	Name of the Co-crystal Structures	Docking Score (kcal/mol)	Docking energy (kcal/mol)	Glide Emodel (kcal/mol)	Binding energy (kcal/mol)	RMSD (nm)
1JIJ	SB-239629	5.412	-34.963	-48.822	-31.21	0.012
1EI1	ANP	-5.290	-38.067	-54.99	-50.07	0.009
1WVG	CXY	-4.302	-41.660	-38.739	-34.003	0.018
2OZ5	OMTS	-6.811	-32.392	-40.221	-41.020	0.093
4OR7	25U	-5.309	-41.720	-51.342	-34.293	0.037

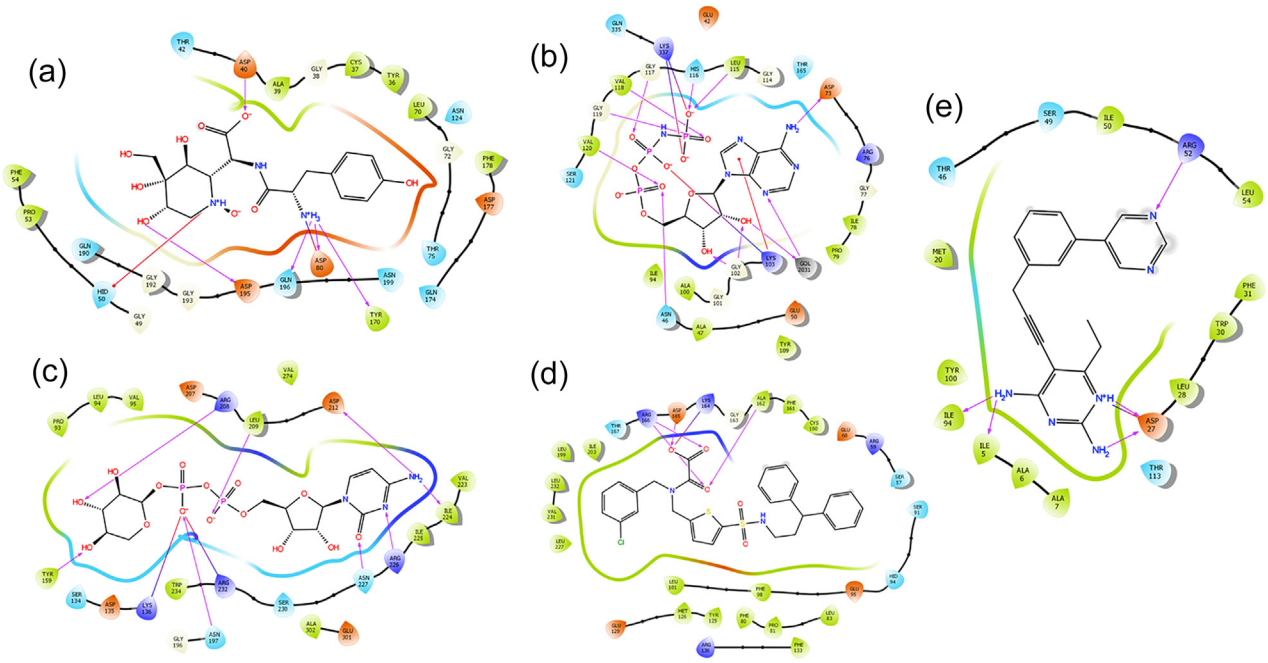

Figure 8. Re-docking interactions of the selected targets with ligands in the respective structures: (a) SB-239629, (b) ANP, (c) CXY, (d) OMTS and (e) 25U.

$[M^+]$ 316, found $[M^+ + 2H]$ 318; calcd. for $C_{16}H_9^{37}Cl_2N_3$: $[M^+]$ 318, found $[M^+ + 2H]$ 320.

Synthesis of 5: Chloroimidazoquinoline **4** (0.71 mmol) and sodium sulphide (1.07 mmol) were dissolved in dimethylformamide and stirred at room temperature for five hours. The reaction mixture was extracted by ethyl acetate and the crude product was purified by silica gel column chromatography with EA:hexane (1:1) to afford the thio-imidazoquinolines **5.**

Compound 5a: yellow colour solid in 82% yield [31]. M.p.: 204–205 °C; ^{1}H NMR (400 MHz, $CDCl_3$) δ: 14.18 (bs, 1H, SH), 9.19 (s, 1H, Ar), 7.98–8.00 (d, J = 8 Hz, 1H, Ar), 7.78–7.80 (d, J = 8 Hz, 1H, Ar), 7.71–7.73 (m, 3H, Ar), 7.41–7.45 (t, J = 8 Hz, 1H, Ar), 7.24–7.27 (m, 2H, Ar) ppm; ^{13}C NMR (125 MHz, DMSO-d_6) δ: 113.24, 115.71, 118.75, 119.62, 120.48, 122.36, 122.74, 123.12, 129.51, 132.06, 134.90, 139.15, 139.53, 143.25, 148.19, 161.26 (C=N) ppm. Anal. calcd for: $C_{16}H_{11}N_3S$: C, 69.29; H, 4.00; N, 15.15%. Found: C, 69.15; H, 3.98; N, 15.18%. HR-MS calcd. for $C_{16}H_{11}N_3S$: $[M^+]$ 277, found $[M + H]^+$ 278.

Compound 5b: 85% yield. M.p.: 224–226 °C; ^{1}H NMR (400 MHz, $CDCl_3$) δ: 14.20 (bs, 1H, SH), 9.21 (s, 1H, Ar), 7.99–8.01 (d, J = 8 Hz, 1H, Ar), 7.70–7.79 (m, 3H, Ar), 7.31–7.46 (m, 3H, Ar), 2.32 (s, 3H, CH_3) ppm. ^{13}C NMR (125 MHz, DMSO-d_6) δ: 22.42, 113.26, 115.74, 118.77, 119.65, 120.49, 122.39, 122.78, 123.16, 129.54, 132.07, 134.97, 139.16, 139.58, 143.26, 148.23, 161.29 (C=N) ppm. Anal. calcd. for: $C_{17}H_{13}N_3S$: C, 70.08; H, 4.50; N, 14.42%. Found: C, 70.18; H, 4.45; N, 14.36%. LC-MS calcd. for $C_{17}H_{13}N_3S$: $[M^+]$ 291, found $[M + H]^+$ 292.

Compound 5c: 79% yield. M.p.: 223–224 °C; ^{1}H NMR (400 MHz, $CDCl_3$) δ: 14.08 (bs, 1H, SH), 9.16 (s, 1H, Ar), 7.95–7.97 (d, J = 8 Hz, 1H, Ar), 7.71–7.82 (m, 2H, Ar), 7.22–7.36 (m, 3H, Ar), 2.48 (s, 3H, CH_3), 2.41 (s, 3H, CH_3) ppm; ^{13}C NMR (125 MHz, DMSO-d_6) δ: 22.41, 22.82, 113.34, 115.81, 118.75, 119.68, 120.52, 122.38, 122.78, 123.16, 129.53, 132.09, 134.94, 139.17, 139.55, 143.29, 148.20, 161.36 (C=N) ppm. Anal. calcd for: $C_{18}H_{15}N_3S$: C, 70.79; H, 4.95; N, 13.76%. Found: C, 70.68; H, 4.91; N, 13.83%. LC-MS calcd. for $C_{18}H_{15}N_3S$: $[M^+]$ 305, found $[M + H]^+$ 306.

Compound 5d: 85% yield. M.p.: 244–245 °C; ^{1}H NMR (400 MHz, $CDCl_3$) δ: 14.28 (bs, 1H, SH), 9.29 (s, 1H, Ar), 8.02–8.04 (d, J = 8 Hz, 1H, Ar), 7.75–7.82 (m, 3H, Ar), 7.27–7.38 (m, 3H, Ar), 3.93 (s, 3H, OCH_3) ppm; ^{13}C NMR (125 MHz, DMSO-d_6) δ: 54.86, 113.34, 115.81, 118.82, 119.65, 120.54, 122.46, 122.78, 123.22, 129.62, 132.12, 134.98, 139.23, 139.61, 143.32, 148.23, 161.29 (C=N) ppm. Anal. calcd for: $C_{17}H_{13}N_3OS$: C, 66.43; H, 4.26; N, 13.67%. Found: C, 66.54; H, 4.28; N, 13.58%. LC-MS calcd. for $C_{17}H_{13}N_3OS$: $[M^+]$ 307, found $[M^+ + 2H]^+$ 309.

Compound 5e: 81% yield. M.p.: 217–220 °C; ^{1}H NMR (400 MHz, $CDCl_3$) δ: 14.29 (bs, 1H, SH), 9.27 (s, 1H, Ar), 7.99–8.01 (d, J = 8 Hz, 1H, Ar), 7.76–7.81 (m, 3H, Ar), 7.32–7.45 (m, 3H, Ar), 3.95 (s, 3H, OCH_3) ppm; ^{13}C NMR (125 MHz, DMSO-d_6) δ: 55.23, 113.32, 115.78, 118.79, 120.05, 120.98, 122.46, 122.84, 123.32, 129.71, 132.36, 134.98, 139.50, 139.59, 143.32, 148.29, 161.46 (C=N) ppm. Anal. calcd for: $C_{17}H_{13}N_3OS$: C, 66.43; H, 4.26; N, 13.67%. Found: C, 66.35; H, 4.18; N, 13.49%. LC-MS calcd. for $C_{17}H_{13}N_3OS$: $[M^+]$ 307, found $[M^+ + 2H]^+$ 309.

Compound 5f: 74% yield. M.p.: 201–202 °C; ^{1}H NMR (400 MHz, $CDCl_3$) δ: 14.38 (bs, 1H, SH), 9.26 (s, 1H, Ar), 7.94–7.96 (d, J = 8 Hz, 1H, Ar), 7.74–7.83 (m, 3H, Ar), 7.27–7.41 (m, 3H, Ar) ppm; ^{13}C NMR (125 MHz, DMSO-d_6) δ: 114.14, 116.73, 119.15, 119.92, 121.82, 122.86, 122.98, 124.13, 130.21, 133.09, 135.80, 139.75, 139.83, 144.35,

149.29, 163.16 (C=N) ppm. Anal. calcd for: $C_{16}H_{10}N_3S$: C, 61.64; H, 3.23; N, 13.48%. Found: C, 61.85; H, 3.14; N, 13.38%. LC-MS calcd. for $C_{16}H_{10}^{35}ClN_3S$: [M^+] 311, found [M + H]$^+$ 312; calcd. for $C_{16}H_{10}^{37}ClN_3S$: [M^+] 313, found [M + H]$^+$ 314.

3.2. Biological studies

3.2.1. Antibacterial activity by agar well diffusion method

The antibacterial activity of the synthesized compounds **3–5(a-f)** was performed on the agar well diffusion method. Each chemical compound was mixed with an equal amount of dimethyl sulfoxide (DMSO) *i.e.,* 1 μl of DMSO contains 1 mg of chemical compound and is considered as the stock solution. The synthesized active chemical compounds were then subjected to the antibacterial activity against the human pathogenic bacteria isolated from Hospital clinical samples which were collected by The Rhizosphere Biology Laboratory, Bharathidasan University, Tiruchirappalli, Tamil Nadu, India. The procured pathogenic bacteria namely *Staphylococcus aureus, Aeromonoas hydrophila, Escherichia coli, Klebsiella pneumonia, Salmonella paratyphi, Salmonella typhi,* and *Mycobacterium butyricum* (MTCC 940) were cultured in nutrient agar medium and incubated at 37 °C for at 16 h. The medium was further used for the antibacterial activity with the synthesized imidazoquinoline derivatives by the agar well diffusion method. Each compound **3–5(a-f)** was poured and checked for their antibacterial activity against the seven collected strains with different concentrations like 10 mg/10 μl, 50 mg/50 μl, and 100 mg/100 μl. The zone of inhibition was found after the incubation period of 24 h at 37 °C and the measurements were reported as diameters in millimeters. The higher zone of inhibition was considered as a significant activity of the synthesized chemical compound against the virulent human pathogenic bacteria [32, 33, 34].

3.2.2. Antioxidant activity using FRAP assay

The antioxidant potential of the imidazoquinolines was examined by using the ferric reducing ability of the plasma FRAP assay. A potent antioxidant could reduce Fe^{3+} to Fe^{2+} and forms a blue complex (Fe^{2+}/TPTZ), which is monitored by UV-vis absorption studies (593 nm). In detail, FRAP reagent was prepared by mixing of acetate buffer (300 μM, pH 3.6), TPTZ (10 μM) in HCl (40 μM) and $FeCl_3$ (20 μM) at 10:1:1 (v/v/v). The sample solutions (10 μl) and reagent (300 μl) were mixed and recorded the absorbance after 10 min. The standard curve was prepared by using Trolox. All the diluted solution results were (Trolox per 100 g dry weight (dw)) performed in triplicates expressed in μM. The stock solutions of each synthesized chemical compound individually mixed with double distilled water about 1 mg/mL and variant concentration about 10 mg/mL were prepared and proceeded the above procedure to react with the FRAP reagents and taken the Optical density level at 593 nm in UV visible spectroscopy. The Optical density was noted and the strength meant its antioxidant potential to control the free radical scavenging activity through standard curve [35, 36].

3.2.3. In silico environment preparation

For this study, the various protein structures from *S. aureus* tyrosyl-tRNA synthetase (1JIJ), *E. coli* -DNA gyrase B (1EI1), *K. pneumoniae* (4OR7), *A. hydrophila* proaerolysin (1PRE), *S. paratyphi* lipopolysaccharide acetyltransferase periplasmic domain (6SE1), *S. typhi* CDP-D-glucose 4, 6-dehydratase (1WVG), *M. tuberculosis* MTB phosphotyrosine phosphatase B protein (2OZ5) are taken for the study. For the desired molecular modeling calculations, the above-mentioned proteins are subjected to the protein preparation wizard implemented in Schrodinger maestro [37]. For the proteins in dimer form, the B chain is removed and the water molecules without interactions are also removed. Using the OPLS-3e forcefield, all the proteins are optimized for their hydrogen atoms and minimized till achieving the least conformation RMSD reaches 0.30Å [38]. Likewise, the ligands **3f**, **4f**, and **5f** were also prepared using the LigPrep [39] molecules for ensuring the correctness of bond orders, ligand charges, and generating conformations up to 32 based on available rotatable bonds. Based on this approach both proteins and ligands are prepared for the molecular modeling environment [40].

3.3. GRID generation and molecular docking

For understanding the molecular interactions of a ligand inside the protein active site, each prepared protein is subject to grid generation using the GLIDE [41]. Before the grid generation, the protein was executed with a sitemap for the active site analysis, and the output of the sitemap generated white dots were manually picked for the Glide Grid generation. As the sitemap didn't predict the active site residues, so the white-colored dot regions and around 2Å radius were considered for active site regions. For each protein Grid generation, the methodology followed was the same, and for that, the white spheres from the sitemap output were manually picked for the XYZ axis. The position of the ligand to be docked was fixed from a 2 Å radius from the site predicted from the sitemap [42]. The generated grid file and prepared ligand files were docked using the XP ligand docking method and validated using Prime MM/GBSA method [43]. Among the ligands, best conformations were scrutinized based on docking score, docking energy, binding energy, and hydrogen bonds formed between the protein-ligand complex.

3.4. Statistical analysis

Statistical analysis was adopted with all parameters exploiting Graphpad prism 7.0 (GraphPad Software, San Diego, CA, USA). Data were represented as the mean ± SD. In column statistics, one sample *t*-test was performed to find the *p*-value (two tailed). The validity of the null hypothesis was verified with a significance level ($\alpha = 0.05$). NS: not significant.

4. Conclusion

In conclusion, we have synthesized the various hydroxyl-, chloro-, and thio-derivatives of imidazoquinolines through a conventional approach in good to moderate yields from the classical intermediate 2-chloro-3-formylquinolines. All the hitherto synthesized imidazoquinolines were screened for their antibacterial activities. Among them, the electron-withdrawing substituent (-Cl) present in the compound **5f** was found to be the most active derivative than other imidazoquinolines, which was comparable with that of the standard. Notably, at high concentration (100 mg/disc), **5f** exhibited the higher activity against *E. coli, K. pneumonia, S. paratyphi, S. typhi, M. butyricum* than that of in standard (10 mg/disc). In addition, other electron-withdrawing and donating substituents containing compounds **4f** and **3f** and **5e** also exhibited moderate activity. The antioxidant power of these compounds was also screened by FRAP. Furthermore, molecular docking studies were carried out for the selected imidazoquinoline derivatives (**3f**, **4f**, and **5f**) with seven types of different proteins. These preliminary results indicated that the antibacterial activity could be enhanced by electron-withdrawing substitution introduced by different positions of the quinoline scaffold. Therefore, these derivatives can be potentially used for MDR antibiotics-related applications.

Declarations

Author contribution statement

K. Velmurugan, Derin Don, S. VishnuPriya: Performed the experiments; Analyzed and interpreted the data; Wrote the paper.

Rajesh Kannan: Performed the experiments; Analyzed and interpreted the data; Contributed reagents, materials, analysis tools or data.

C. Selvaraj: Analyzed and interpreted the data; Wrote the paper.

G. Selvaraj: Analyzed and interpreted the data.

S.K. Singh: Analyzed and interpreted the data; Contributed reagents, materials, analysis tools or data.

R. Nandhakumar: Conceived and designed the experiments; Contributed reagents, materials, analysis tools or data.

Funding statement

This work was supported by RUSA-Phase 2.0 Policy (TNmulti-Gen), Dept. of Edn, Govt. of India (Grant No: F.24-51/2014-U).

Data availability statement

Data included in article/supplementary material/referenced in article.

Declaration of interests statement

The authors declare no conflict of interest.

Additional information

No additional information is available for this paper.

References

[1] M.A. Brockhurst, F. Harrison, J.W. Veening, E. Harrison, G. Blackwell, Z. Iqbal, C. Maclean, Assessing evolutionary risks of resistance for new antimicrobial therapies, Nat. Ecol. Evol. 3 (2019) 515–517.
[2] V. Cattoir, B. Felden, Future antibacterial strategies: from basic concepts to clinical challenges, J. Infect. Dis. 220 (2019) 350–360.
[3] https://www.cdc.gov/drugresistance/biggest-threats.html.
[4] S.S. Pandit, R.K. Mahesh, B.P. Yashwant, P.L. Nitin, M.K. Vijay, Synthesis and in vitro evaluations of 6-(hetero)-aryl-imidazo [1, 2-b] pyridazine-3-sulfonamide's as an inhibitor of TNF-α production, Bioorg. Med. Chem. Lett 28 (2018) 24–30.
[5] A.K. Bagdi, S. Sougata, M. Kamarul, H. Alakananda, Synthesis of imidazo[1, 2-a] pyridines: a decade update, Chem. Commun. 51 (2015) 1555–1575.
[6] E.D. Brown, G.D. Wright, Antibacterial drug discovery in the resistance era, Nature 529 (2016) 336–343.
[7] R. Voelker, Antibacterial inhibits resistance, J. Am. Med. Assoc. 318 (2017) 1432.
[8] A. Dorababu, Recent update on antibacterial and antifungal activity of quinoline scaffolds, Arch. Pharm. (2020), e2000232.
[9] X.F. Zheng, C.G. Liang, L.S. Wang, B.X. Wang, Y.F. Liu, S. Feng, J.Z. Wu, L. Gao, L.C. Feng, L. Chen, T. Guo, H.C. Shen, H.Y. Yun, Discovery of benzoazepinequinoline (BAQ) derivatives as novel, potent, orally bioavailable respiratory syncytial virus fusion inhibitors, J. Med. Chem. 61 (2018) 10228–10241.
[10] M.M. Al-Sanea, A. Elkamhawy, S. Paik, K. Lee, A.M. El Kerdawy, B.S.N. Abbas, E.J. Roh, W.M. Eldehna, H.A.H. Elshemy, R.B. Bakr, I.A. Farahat, A.I. Alzarea, S.I. Alzarea, K.S. Alharbi, M.A. Abdelgawad, Sulfonamide-based 4-anilinoquinoline derivatives as novel dual Aurora kinase (AURKA/B) inhibitors: synthesis, biological evaluation and in silico insights, Bioorg. Med. Chem. 28 (2020) 115525.
[11] K. Muthukumar, K. Velmurugan, T.D. Derin, P. Rajesh, V. Rajesh Kannan, R. Nandhakumar, Synthesis, characterization, antibacterial and antioxidant studies of oxetoquinolines, MOJ Biorg. Org. Chem. 3 (2019) 38–43.
[12] M. Baumann, I.R. Baxendale, A continuous-flow method for the desulfurization of substituted thioimidazoles applied to the synthesis of etomidate derivatives, Eur. J. Org Chem. 2017 (2017) 6518–6524.
[13] S.M. Gomha, M.M. Edress, Z.A. Muhammad, H.M. Gaber, M.M. Amin, I.K. Matar, Synthesis under microwave irradiation and molecular docking of some novel bioactive thiadiazoles, Mini Rev. Med. Chem. 19 (2019) 437–447.
[14] J.R. Hunt, P.A. Kleindl, K.R. Moulder, T.E. Prisinzano, M.L. Forrest, Further exploration of the structure-activity relationship of imidazoquinolines; identification of potent C7-substituted imidazoquinolines, Bioorg. Med. Chem. Lett 30 (2020) 126788.
[15] S. Jangra, J.D. Vrieze, A. Choi, R. Rathnasinghe, G. Laghlali, A. Uvyn, S.V. Herck, L. Nuhn, K. Deswarte, Z. Zhong, N.N. Sanders, S. Lienenklaus, S.A. David, S. Strohmeier, F. Amanat, F. Krammer, H. Hammad, B.N. Lambrecht, L. Coughlan, A. García-Sastre, B.G.D. Geest, M. Schotsaert, Sterilizing immunity against SARS-CoV-2 infection in mice by a single-shot and lipid amphiphile imidazoquinoline TLR7/8 agonist-adjuvanted recombinant spike protein vaccine, Angew. Chem. Int. Ed. 60 (2021) 9467–9473.
[16] D. Ao, X. Liu, P. Xia, H. Wang, S. Jiang, W. Zheng, N. Chen, F. Meurens, J. Zhu, Identification of imidazoquinoline derivative (IQD) interacting sites of porcine TLR8 and the underlying species specificity, Mol. Immunol. 136 (2021) 45–54.
[17] Z. Xiao, F. Lei, X. Chen, X. Wang, L. Cao, K. Ye, W. Zhu, S. Xu, Design, synthesis, and antitumor evaluation of quinoline-imidazole derivatives, Arch. Pharm. Chem. Life Sci. (2018), e1700407.
[18] S. Kwon, Y. Lee, Y. Jung, J.H. Kim, B. Baek, B. Lim, J. Lee, I. Kim, J. Lee, Mitochondria-targeting indolizino[3,2-c]quinolines as novel class of photosensitizers for photodynamic anticancer activity, Eur. J. Med. Chem. 148 (2018) 116–127.
[19] N.B. Ghate, D. Chaudhuri, S. Panja, S.S. Singh, G. Gupta, C.Y. Lee, N. Mandal, In vitro mechanistic study of the anti-inflammatory activity of a quinoline isolated from spondias pinnata bark, J. Nat. Prod. 81 (2018) 1956–1961.
[20] B. Ezraty, A. Gennaris, F. Barras, J.-F. Collet, Oxidative stress, protein damage and repair in bacteria, Nat. Rev. Microbiol. 15 (2017) 385–396.
[21] D. Verbanac, R. Malik, M. Chand, K. Kushwaha, M. Vashist, M. Matijasic, V. Stepanic, M. Peric, H.C. Paljetak, L. Saso, S.C. Jain, Synthesis and evaluation of antibacterial and antioxidant activity of novel 2-phenyl-quinoline analogs derivatized at position 4 with aromatically substituted 4H-1,2,4-triazoles, J. Enzym. Inhib. Med. Chem. 31 (2016) 104–110.
[22] J.P.S. Ferreira, S.M. Cardoso, F.A.A. Paz, A.M.S. Silva, V.L.M. Silva, Synthesis of 2-aroylfuro[3,2-c]quinolines from quinolone-based chalcones and evaluation of their antioxidant and anticholinesterase activities, New J. Chem. 44 (2020) 6501–6509.
[23] B. Muddam, P. Venkanna, M. Venkateswarlu, M.S. Kumar, K.C. Rajanna, Symmetrical trichlorotriazine derivatives as efficient reagents for one-pot synthesis of 3-Acetyl-2-chloroquinolines from acetanilides under vilsmeier-haack conditions, Synlett 29 (2018) 85–88.
[24] R. Nandhakumar, T. Suresh, T. Dhanabal, P.S. Mohan, Utility of Vilsmeier Haack reagent in the synthesis of 3-amino-12-chloro quino[3,2-e][1,3]diazocines, Indian J. Chem. 43B (2004) 846–851.
[25] K. Velmurugan, J. Prabhu, L. Tang, T. Chidambaram, M. Noel, S. Radhakrishnan, R. Nandhakumar, A simple chalcone-based fluorescent chemosensor for the detection and removal of Fe^{3+} ions using a membrane separation method, Anal. Methods 6 (2014) 2883–2888.
[26] K. Velmurugan, R. Vickram, C.V. Jipsa, R. Karthick, G. Prabakaran, S. Suresh, J. Prabhu, G. Velraj, L. Tang, R. Nandhakumar, Quinoline based reversible fluorescent probe for Pb^{2+}; applications in milk, bioimaging and INHIBIT molecular logic gate, Food Chem. 348 (2021) 129098.
[27] R.M. Abdelhameed, O.M. Darwesh, M. El-Shahat, Synthesis of arylidene hydrazinylpyrido[2,3-d]pyrimidin-4-ones as potent anti-microbial agents, Heliyon 6 (2020), e04956.
[28] E.M. Flefel, W.I. El-Sofany, M. El-Shahat, A. Naqvi, E. Assirey, Synthesis, molecular docking and in vitro screening of some newly synthesized triazolopyridine, pyridotriazine and pyridine–pyrazole hybrid derivatives, Molecules 23 (2018) 2548.
[29] M. Sankaran, C. Kumarasamy, U. Chokkalingam, P.S. Mohan, Synthesis, antioxidant and toxicological study of novel pyrimido quinoline derivatives from 4-hydroxy-3-acyl quinolin-2-one, Bioorg. Med. Chem. Lett 20 (2010) 7147–7151.
[30] K. Velmurugan, A. Raman, D. Derin, L. Tang, S. Easwaramoorthi, R. Nandhakumar, Quinoline benzimidazole-conjugate for the highly selective detection of Zn(II) by dual colorimetric and fluorescent turn-on responses, RSC Adv. 5 (2015) 44463–44469.
[31] K. Velmurugan, A. Thamilselvan, R. Antony, V.R. Kannan, L. Tang, R. Nandhakumar, Imidazoloquinoline bearing thiol probe as fluorescent electrochemical sensing of Ag and relay recognition of Proline, J. Photochem. Photobiol. Chem. 333 (2017) 130–141.
[32] M. Desai, M. Beall, M.G. Ross, Developmental origins of obesity: programmed adipogenesis, Curr. Diabetes Rep. 13 (2013) 27–33.
[33] S. Gogoi, K. Shekarrao, A. Duarah, T.C. Bora, S. Gogoi, R.C. Boruah, A microwave promoted solvent-free approach to steroidal quinolines and their in vitro evaluation for antimicrobial activities, Steroids 77 (2012) 1438–1445.
[34] N.A.N.N. Malek, N.S. Malek, Modification of synthetic zeolites by quaternary ammonium compounds and its antibacterial activity against Bacillus subtilis, APCBEE Proc. 3 (2012) 134–139.
[35] M. Antolovich, P. Prenzler, E. Patsalides, Methods for testing antioxidant activity, Analyst 127 (2002) 183–198.
[36] D. Kaushik, A. Kumar, P. Kaushik, A.C. Rana, Analgesic and anti-inflammatory activity of *Pinus roxburghii sarg*, Adv. Pharmacol. Sci. 2012 (2012) 245431.
[37] Schrödinger Release 2021-2: Protein Preparation Wizard, Epik, Schrödinger, LLC, New York, NY, 2021. Impact, Schrödinger, LLC, New York, NY; Prime, Schrödinger, LLC, New York, NY, 2021.
[38] G.M. Sastry, M. Adzhigirey, T. Day, R. Annabhimoju, W. Sherman, Protein and ligand preparation: parameters, protocols, and influence on virtual screening enrichments, J. Comput. Aided Mol. Des. 27 (2013) 221–234.
[39] Schrödinger Release 2021-2, LigPrep, Schrödinger, LLC, New York, NY, 2021.
[40] C. Selvaraj, U. Panwar, D.C. Dinesh, E. Boura, P. Singh, V.K. Dubey, K.S. Singh, Microsecond MD simulation and multiple-Confirmation virtual screening to identify potential anti-COVID-19 inhibitors against SARS-CoV-2 main protease, Front. Chem. 8 (2020) 1179.
[41] Schrödinger Release 2021-2: Glide, Schrödinger, LLC, New York, NY, 2021.
[42] R.A. Friesner, J.L. Banks, R.B. Murphy, T.A. Halgren, J.J. Klicic, D.T. Mainz, M.P. Repasky, E.H. Knoll, D.E. Shaw, M. Shelley, J.K. Perry, P. Francis, P.S. Shenkin, Glide: a new approach for rapid, accurate docking and scoring. 1. Method and assessment of docking accuracy, J. Med. Chem. 47 (2004) 1739–1749.
[43] Schrödinger Release 2021-2: Prime, Schrödinger, LLC, New York, NY, 2021.